Catalysis Today 168 (2011) 63–70

Contents lists available at ScienceDirect

Catalysis Today

journal homepage: www.elsevier.com/locate/cattod

Post-synthesis modification of TUN zeolite: Textural, acidic and catalytic properties

Martin Kubů [a], Naděžda Žilková [a], Jiří Čejka [a,b,*]

[a] J. Heyrovský Institute of Physical Chemistry, Academy of Sciences of the Czech Republic, v.v.i., Dolejškova 3, CZ-182 23 Prague 8, Czech Republic
[b] Center of Excellence in Refining and Petrochemistry, King Fahd University of Petroleum & Minerals, Dhahran 31261, Saudi Arabia

ARTICLE INFO

Article history:
Received 5 October 2010
Received in revised form
26 November 2010
Accepted 29 November 2010
Available online 12 January 2011

Keywords:
TUN
Dealumination
Desilication
Hierarchic system
Aromatic transformations
Internal and external acidity

ABSTRACT

Dealumination, desilication and silylation of TUN zeolite was investigated and related to the catalytic behavior in toluene disproportionation and its alkylation with isopropyl alcohol. Only negligible concentration of acid sites was identified on the "external" surface of parent TUN zeolite and this concentration increased with increasing desilication. Silylation resulted in channel narrowing and probably some plugging. As a result, significant increase in the *para*-selectivity in toluene disproportionation and its alkylation with isopropyl alcohol was achieved. No changes in toluene conversion were observed for all parent and modified samples in toluene alkylation confirming diffusion and transport of products as the rate determining step in 10-ring zeolites. Selectivity to cymenes and *p*-cymene decreased with dealumination as well as desilication. In contrast, silylation increased both cymene (80%) and *p*-cymene (90%) selectivity in toluene alkylation.

1. Introduction

Zeolites represent one of the most important groups of heterogeneous catalysts with numerous applications in chemical industry [1–3]. The interplay among textural, chemical and catalytic properties is optimized for a high performance in these processes. Despite that zeolites generally suffer from a low accessibility of acid sites located in micropore channels for bulkier reactants.

One of the possible ways to overcome low accessibility is the fabrication of hierarchical zeolites, it means those successfully combining micropores and mesopores. Such systems are much more flexible and transport of bulky reactants and products proceeds with a higher efficiency [4,5]. Dealumination and particularly desilication were recently intensively investigated to provide mesopores in different structural types of zeolites. MFI [6], MOR [7], FER [8], MWW [9], IFR [10], and STF [11] are some examples of successful desilication. Desilication not only increased significantly the mesoporosity of these hierarchic zeolites but also changed the acidic properties by removing a part of silica material. Therefore, it is believed that optimum combination of post-synthesis treatment with appropriate zeolite type can provide a highly efficient zeolite-based catalyst [4,5].

Recently, diquaternary ammonium structure directing-agents (SDA) built from N-methyl pyrrolidine heterocycles connected by methylene chain of different lengths [12] led to the discovery of novel zeolites -SVR [13], IMF [14] and TUN [15]. Their structures are rather complex and were recently finally solved [16–18]. TUN is a new high-silica zeolite possessing 24 crystallographically distinct tetrahedral sites (T-sites) in its monoclinic unit cell. Its framework contains two distinct straight 10-ring channels (0.52 nm × 0.60 nm and 0.51 nm × 0.55 nm). TUN crystallizes under hydrothermal conditions at the expense of a lamellar precursor over a very narrow range of Si/Al and $NaOH/SiO_2$ ratios. The proton form of TUN exhibits high hydrothermal stability, strong acidity and unique shape selective properties in acid-catalyzed reactions of monoaromatic hydrocarbons (benzene and toluene alkylation, disproportionation of toluene and isomerization of *m*-xylene [15,19,20]) or cracking of vacuum gas–oil [21].

This contribution focuses on the post-synthesis treatments of TUN zeolite via dealumination, desilication and silylation. Textural, acidic, and catalytic properties of parent and modified TUN samples were investigated. The relationship between acidity (both internal and external) and catalytic activity in toluene disproportionation and its alkylation with isopropyl alcohol is discussed as well.

* Corresponding author.
E-mail address: Jiri.cejka@jh-inst.cas.cz (J. Čejka).

0920-5861/$ – see front matter © 2011 Published by Elsevier B.V.
doi:10.1016/j.cattod.2010.11.090

2. Experimental

2.1. Synthesis

TUN zeolite was synthesized according to Ref. [15]. $AlCl_3 \cdot 6H_2O$ (>99%, Fluka) was used as a source of aluminum and fumed silica (Aldrich) as a source of silica. The organic SDA cation 1,4-bis(N-methylpyrrolidinium) butane (1,4-MPB) was prepared according to the literature [22]. The synthesis was carried out under agitation in 90-mL Teflon-lined stainless steel autoclaves heated at 160 °C and autogenous pressure for 12 days. After that, the autoclaves were cooled down to the ambient temperature, the solid product was filtered off, washed out with excess of distilled water and dried in the oven at 80 °C overnight. As-made TUN zeolite was calcined under flowing air at 580 °C for 12 h with a heating rate 1 °C/min. Calcined TUN sample was then treated four-times with 1.0 M NH_4NO_3 solution (99%, Lach-Ner) for 4.5 h at room temperature using 100 mL of solution per 1 g of zeolite. Ammonium forms of TUN samples were activated before each measurement to remove ammonia and to provide proton form of the zeolite.

2.2. Post-synthesis treatments

Ammonium form of TUN was calcined under flowing air at 450 °C with a heating rate 10 °C/min to obtain H^+ form of zeolite. Dealumination was performed via treatment with different concentrated solution of HNO_3 (Lachema, CZE) at 100 °C under reflux using 25 mL/g of zeolite. After that, the solid product was recovered by filtration, washed with distilled water until neutral pH was reached and finally dried overnight at 60 °C.

Desilication procedure was based on Ref. [23]. In 100-mL flask, 2.5 g of TUN was stirred in 77 mL of 0.2 M NaOH aqueous solution (Lach-Ner) at 65 °C under reflux for different periods of time (Table 1). Subsequently, the flask was cooled down, the solid product was filtered and washed out with distilled water to reach neutral pH and then dried at 60 °C overnight. Na^+ form of TUN was converted to NH_4^+ form by four-fold treatment with 1.0 M NH_4NO_3 solution at room temperature for 4.5 h.

The silylation procedure proceeded in this way: ammonium form of TUN was activated in argon stream at 450 °C with a heating rate 10 °C/min for 2 h followed by cooling to ambient temperature under argon. Dry toluene (25 mL/g of zeolite) and defined amount of tetraethyl orthosilicate (TEOS, 1.0 wt.%, Aldrich) were added with exclusion of air moisture. Afterwards, the mixture was stirred at room temperature overnight, followed by heating under reflux for 4 h. Evaporation of liquid phase in vacuum closed the procedure. The silylated sample was calcined in air at 450 °C for 8 h. Table 1 summarizes the abbreviations of all samples studied and the conditions of post-synthesis treatments applied.

2.3. Characterization

The crystallinity of all TUN samples was checked by powder X-ray diffraction (XRD) using a Bruker AXS D8 Advance diffractometer with a graphite monochromator and a position sensitive detector Våntec-1 using CuKα radiation in Bragg–Brentano geometry. The size and shape of zeolite crystals were examined by scanning electron microscopy (SEM) on a JEOL, JSM-5500LV microscope. For the measurement, crystals were coated with a thin platinum layer by sputtering in vacuum chamber of a BAL-TEC SCD-050.

For the determination of the chemical composition of synthesized and modified zeolites, X-ray fluorescence analysis with a Philips PW 1404 spectrometer equipped with an analytical program UniQuant was used. The samples were mixed with dentacryl as a binder and pressed on the surface of cellulose pellets.

Concentration of Lewis (L) and Brønsted (B) acid sites was determined after adsorption of pyridine (PYR) by FTIR spectroscopy (Nicolet Protégé 460 Magna). Zeolites were pressed into self-supporting wafers with a density of 8.0–12 mg/cm^2 and activated in situ at 450 °C overnight. Before adsorption pyridine was degassed by freezing and thawing cycles. Pyridine adsorption was carried out at 150 °C for 20 min at partial pressure 600–800 Pa, followed by desorption for 20 min. All spectra were recorded with a resolution of 2 cm^{-1} by collecting 128 scans for a single spectrum at room temperature. Spectra were recalculated on wafer density of 10 mg/cm^2. Concentration of Lewis and Brønsted acid sites were evaluated from the integral intensities of bands at 1454 cm^{-1} (Lewis acid sites) and at 1545 cm^{-1} (Brønsted acid sites) using extinction coefficients, ε (L) = 2.22 cm/μmol, and ε (B) = 1.67 cm/μmol [24].

The adsorption of 2,6-di-tert-butylpyridine (DTBP) took place at 150 °C, and at equilibrium probe vapour pressure with the zeolite wafer for 15 min. Desorption proceeded at the same temperature for 1 h followed by collection of spectra at room temperature. Extinction coefficients for pyridine [24] were used for the quantitative analysis evaluation of the concentration of Lewis and Brønsted acid sites.

Nitrogen sorption isotherms were measured on a Micromeritics ASAP 2020 volumetric instrument at liquid nitrogen temperature (−196 °C) to determine surface area, pore volume and pore size distribution of TUN. Prior to the sorption measurements, all samples were degassed at 250 °C for at least 24 h. Detailed description can be found in [25].

2.4. Catalytic experiments

The disproportionation and alkylation of toluene with isopropyl alcohol were investigated in a down-flow glass microreactor with a fixed bed of catalyst under atmospheric pressure. Zeolite catalyst was pressed and sieved and the fraction between 0.750 and 0.355 mm was used for the reaction. Before the catalytic run, zeolite catalysts were activated at 500 °C in nitrogen stream for 120 min.

Table 1
Experimental conditions of post-synthesis treatment and respective textural properties.

Marking	HNO_3 conc. (M)	NaOH conc. (M)	Si (wt.%)	Time (h)	V_{mic} (cm^3/g)	V_{meso} (cm^3/g)	S_{BET} (m^2/g)	Δw (%)[a]
TUN	–	–	–	–	0.167	–	418	–
TUN/A	0.5	–	–	2	0.172	–	442	–
TUN/B	1.0	–	–	2	0.168	–	430	–
TUN/C	6.0	–	–	2	0.169	–	429	–
TUN/D	–	0.2	–	0.25	0.141	0.234	435	12.7
TUN/E	–	0.2	–	0.5	0.140	0.298	473	27.7
TUN/F	–	0.2	–	2	0.133	0.340	474	42.6
TUN/G	–	–	1.0[b]	–	0.160	–	406	–

[a] Weight reduction after desilication.
[b] TEOS.

The disproportionation of toluene was carried out at 450 and 500 °C with WHSV 1.9 and 18.9 h^{-1}. The alkylation of toluene was performed at 250 °C and toluene to isopropyl alcohol molar ratio of 9.6 and weight hour space velocity (WHSV) based on toluene equal to 10 h^{-1}.

The reaction products were analyzed using an "on-line" gas chromatograph (Agilent 6890 Plus) with flame ionization detector and a high-resolution capillary column (Innowax for the disproportionation and DB-5 for the alkylation). The first analysis was performed after 15 min of time-on-stream (T-O-S) and the other followed in approx. 55 min interval.

3. Results and discussion

3.1. Characterization of TUN zeolites

Combination of different experimental techniques has been applied to characterize in detail the chemical and textural properties of parent and post-synthetically modified TUN zeolites. Fig. 1 shows X-ray diffraction patterns of parent TUN zeolite and TUN modified by dealumination, desilication and surface silylation. All four X-ray patterns evidence high crystallinity and phase purity of these samples confirming that no structural changes proceeded during the post-synthesis treatments. The same XRD patterns were obtained also for remaining TUN samples under study (not shown here).

Scanning electron images of parent and modified TUN zeolites are given in Fig. 2 under the same resolution. From the images it is seen that the size of TUN crystals is about 2 μm × 1 μm × 1 μm with a few larger agglomerates. There is no sign of another phase or amorphous species in the TUN zeolite. The applied synthesis resulted in rather homogeneous distribution of crystals sizes and shapes of TUN zeolites. The size and shape is practically not changed after individual modification treatments. Neither dealumination, nor desilication and nor silylation led to dramatic changes of the crystals habitus.

Nitrogen adsorption isotherms provided valuable information on the textural properties of individual TUN samples when compared with the parent zeolite (cf. Fig. 3A and Table 1). Samples TUN/A, TUN/B and TUN/C were prepared by dealumination carried out under reflux for 2 h by varying the concentration of nitric acid. The adsorption isotherms did not practically change their shape and all samples posses practically the same micropore volume (0.167–0.172 cm^3/g), which is the value confirming a high quality of the TUN samples studied (Table 2). The silylation treatment led to a little decrease in the micropore volume as well as BET surface area. Thus, we can expect that silica material used for modification is mainly located on the external surface or in channel entrances of TUN crystals without a significant penetration into the TUN channel system. Results differ from those obtained on STF zeolite [11] where a substantial decrease in the micropore volume after the silylation was reported. The main reason is probably a special structure of STF zeolite with individual 18-ring STF cages being separated by only one 10-ring. Thus, larger molecules can more easily penetrate to the channel system of STF despite 1D channel structure.

In contrast, desilication changed significantly the textural properties of TUN zeolites. With increasing time of the treatment at the same concentration of NaOH (Table 1) micropore vol-

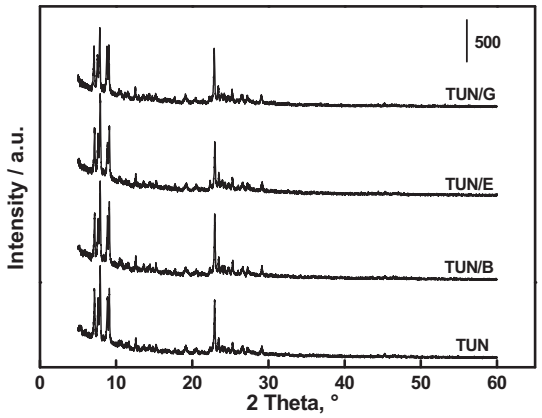

Fig. 1. XRD patterns of TUN.

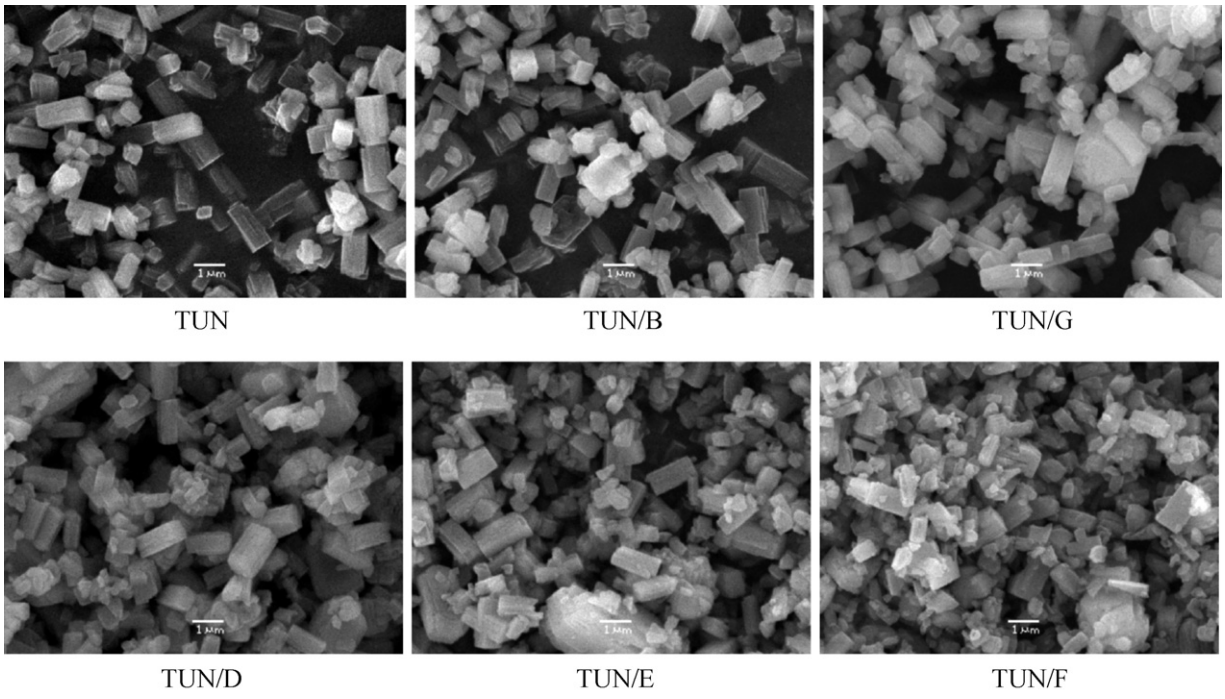

Fig. 2. SEM images of parent and treated TUN.

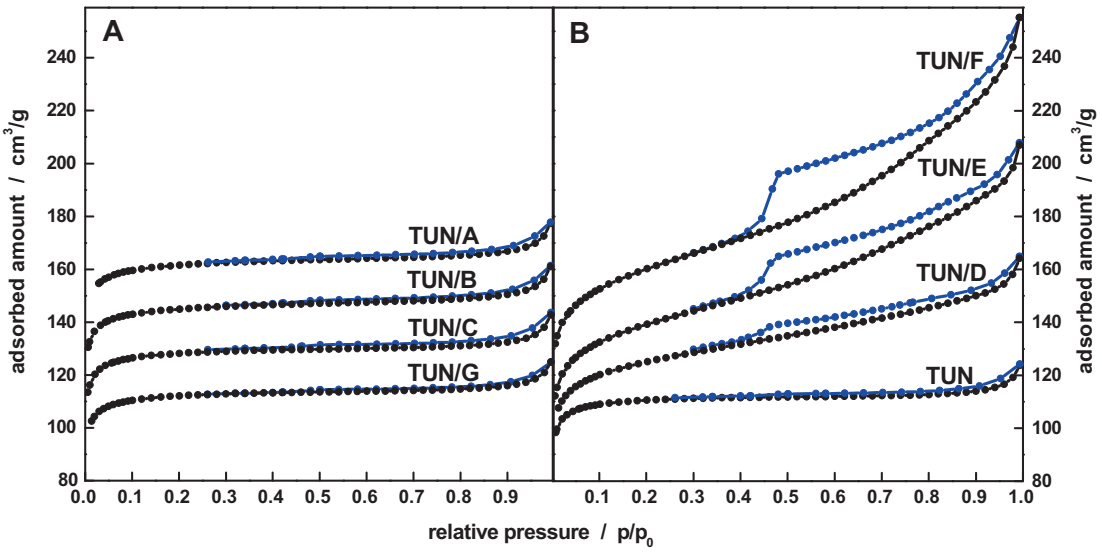

Fig. 3. Nitrogen isotherms. Dealuminated and silylated TUN (A), parent and desilicated (B). For better view, following isotherms were shifted along *y* axis (in cm^3/g): TUN/G +0,TUN/C +10, TUN/B +25, TUN/A +40 (A), TUN −5, TUN/D +5, TUN/E +10, TUN/F +30 (B).

ume decreased very slightly, however, volume of mesopores and BET areas increased dramatically. After 0.25 h mesopore volume reached the value 0.234 cm^3/g and after 2 h 0.340 cm^3/g was achieved. In parallel, BET surface area increased from 418 (parent TUN) to 474 (TUN/F). Formation of mesopores is nicely visible from the shape of the adsorption isotherms exhibiting large hysteresis loop, the size of which increases with prolongation of the time of desilication (Fig. 3B). The shape of the hysteresis loop evidences a broad range of mesopores of different sizes and shapes. Desilication treatment was accompanied by a large weight loss reaching 42.6 wt.% after 2 h of desilication treatment.

3.2. Acidic properties of TUN zeolites

With relation to the catalytic behavior of TUN zeolite and its modified analogues, acidity assessment is of critical importance. To understand in more detail the acidic properties of zeolites studied, the concentration and type of acid sites were studied using FTIR with pyridine and 2,6-di-tert-butyl-pyridine as probe molecules [26–29]. The infrared spectra of parent TUN zeolite (Fig. 4A) exhibit three absorption bands in the region of hydroxyl vibrations, more specifically, a band at 3745 cm^{-1} belonging to terminal silanol groups, a relatively weak absorption band at 3670 cm^{-1} due to the presence of OH groups attached to extra-framework alumina species and finally strong absorption band at 3610 cm^{-1} assigned to acidic bridging Si–OH–Al groups [30].

Pyridine absorption on parent TUN and all modified TUN samples resulted in complete disappearance of the absorption band of Si–OH–Al groups and that of OH groups attached to extra-framework alumina (Fig. 4A, C and E). This confirms that all Brønsted acid sites in TUN regardless the way of modification are accessible for pyridine. In the region of pyridine vibration bands of pyridine interacting with Brønsted and Lewis acid sites appeared. Absorption band at 1545 cm^{-1} is characteristic for pyridine interacting with Brønsted acid sites while bands around 1450 cm^{-1} are attributed to pyridine being in interaction with Lewis acid sites or silanol groups (Fig. 4B, D and F). Extinction coefficients and integral areas of these bands have been used to quantitatively determine the concentrations of individual sites according to Ref. [26].

Dealumination procedure resulted in a slight decrease in the concentration of Lewis acid sites while concentration of Brønsted sites remained practically unchanged (Fig. 4E and F). It is in a good agreement with only a slight increase in Si/Al ratio. The concentration of Brønsted and Lewis acid sites was changed very slightly (Table 2). This dealumination procedure under the same conditions was recently applied for STF zeolites possessing Si/Al ratio 29 [11]. STF exhibited much larger extent of dealumination when compared with TUN although having a higher Si/Al ratio. One can speculate about a higher resistance to acidic treatment in the case of TUN zeolite. Interaction of 2,6-di-tert-butyl-pyridine with parent and dealuminated TUN samples showed only a negligible concentration of accessible Brønsted sites (Fig. 5B and F). It evidences that practically no acid sites are located on the external surface or mouth openings and expectedly dealuminated samples are also almost without acid sites on the crystal surface (Table 2).

In contrast, silylated TUN/G possesses substantially lowered concentration of Brønsted sites (from 0.35 to 0.20 mmol/g) while the decrease in the amount of Lewis acid sites was smaller (0.22–0.17 mmol/g). No acid sites were distinguished on the external surface after silylation and the increase in Si/Al ratio cor-

Table 2
Lewis and Brønsted acid site concentration. Adsorption of pyridine and 2,6-di-tert-butylpyridine (I).

Marking	Si/Al	c_B (mmol/g)	c_L (mmol/g)	c_B (%)	c_L (%)	c_B (I) (mmol/g)	Si/Al (CA)
TUN	20.2	0.35	0.22	62	38	–	16.1
TUN/A	21.9	0.34	0.20	63	37	–	16.3
TUN/B	22.2	0.34	0.19	65	35	–	16.5
TUN/C	23.0	0.34	0.18	66	34	–	17.9
TUN/D	16.7	0.30	0.32	49	51	0.026	13.8
TUN/E	16.4	0.29	0.33	46	54	0.033	12.5
TUN/F	15.8	0.28	0.33	44	56	0.038	11.3
TUN/G	22.4	0.20	0.17	55	45	–	16.4

CA, chemical analysis.

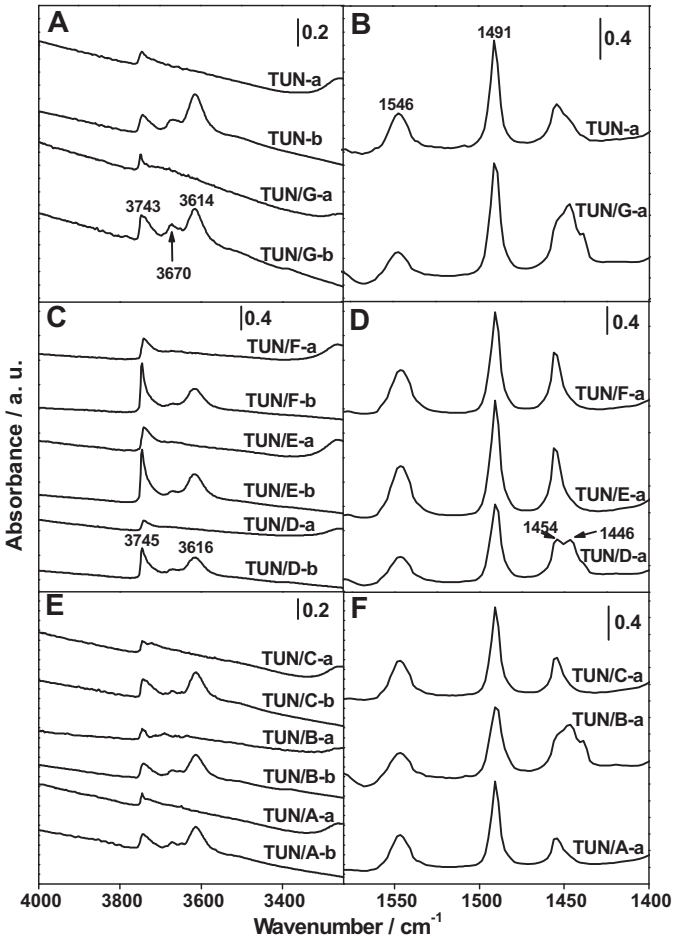

Fig. 4. FTIR spectra of TUN. Adsorption of pyridine. Region of hydroxyl vibration (A, C and E), region of pyridine vibration (B, D and F). After (a) and before (b) adsorption.

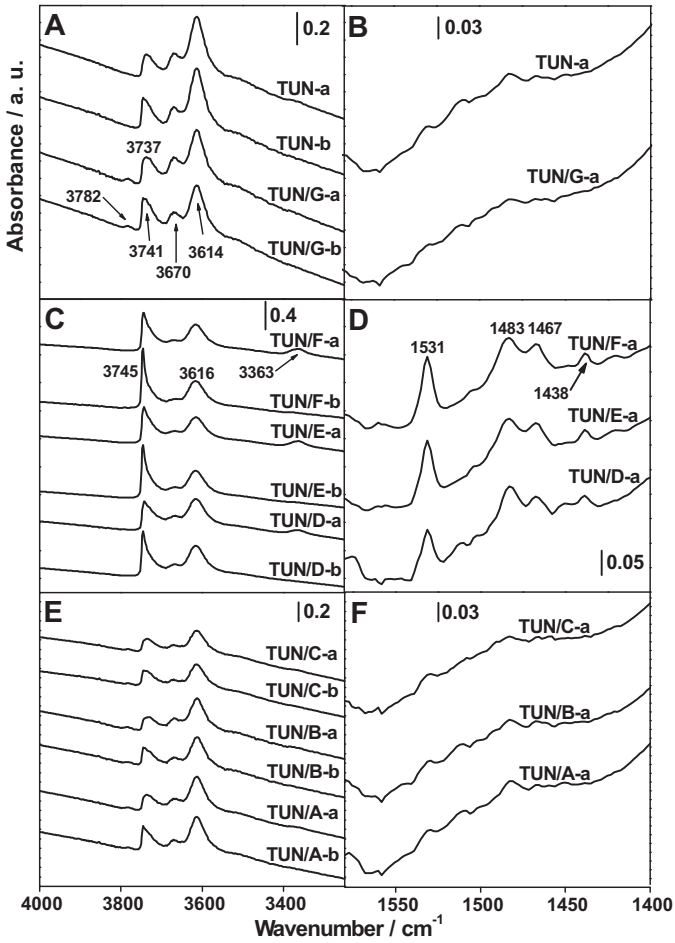

Fig. 5. FTIR spectra of TUN. Adsorption of 2,6-di-tert-butylpyridine. Region of hydroxyl vibration (A, C and E), region of 2,6-di-tert-butylpyridine vibration (B, D and F). After (a) and before (b) adsorption.

responds to the amount of Si added during the post-synthesis treatment (Table 1). It indicates that silylation closed or narrowed some channel entrances and pyridine is no longer able to reach the acid sites. It is supported by only a slight decrease in micropore volume (0.167 cm^3/g for TUN and 0.160 cm^3/g for TUN/G).

Desilication led not only to the substantial increase in the mesopore volume (Table 1) but also to substantial changes in the concentration of acid sites and their location. Concentration of Brønsted sites decreased from 0.35 to 0.28–0.30 mmol/g depending on the length of treatment but simultaneously the desilication led to an increase in the concentration of Lewis acid sites from 0.22 to 0.33 mmol/g. Consequently, higher concentrations of Lewis acid sites were observed than of Brønsted sites. Fig. 5C and D shows spectra of desilicated samples before and after adsorption of 2,6-di-tert-butyl-pyridine and adsorbed 2,6-di-tert-butyl-pyridine on Brønsted acid sites, their concentrations are provided in Table 2. Absorption band at 1531 cm^{-1} is typical for interaction of 2,6-di-tert-butyl-pyridine with Brønsted acid sites and the absence of a band at 1545 cm^{-1} confirms no dealkylation of the probe molecules used. The concentration of acid sites on the external surface of zeolite crystals increases with prolongation of the desilication treatment and simultaneously with increasing mesopore volume. As the differences in mesopore volume and weight loss during the desilication treatment for individual TUN samples are substantial in contrast to a slight increase in the concentration of Brønsted sites at the external surface, it can be inferred that there could be a large siliceous domains in the structure of TUN zeolite. Desilication then results in the removal of silica from these domains while the surface composition is not significantly changed.

3.3. Catalytic behavior of TUN zeolites

In addition to the general interest in textural and acidic properties of micro/mesoporous zeolites we tried also to evaluate their effects on the catalytic behavior in different reactions. Transformations of aromatic hydrocarbons are particularly sensitive to textural/structural and acidity changes as documented in numerous literature [2,3,31–33].

Toluene disproportionation belongs to the reactions, the rate of which is supposed to be controlled by the concentration of acid sites even in the case of medium-pore zeolites [3]. MFI is the only zeolite being able to provide *para*-selectivity higher than that related to the thermodynamic equilibrium due to the transport phenomena. Therefore, this reaction was chosen for comparison of parent and post-synthesis modified TUN zeolite.

Surprisingly, no big differences in toluene conversions in its disproportionation were obtained for parent and modified TUN zeolites at 450 °C (Fig. 6A) and 500 °C (not shown here). This is most probably related to similar concentrations of acid sites and it indicates that diffusion is not a critical factor. These results are in contrast to recently reported behavior of mesoporous ZSM-5 zeolites prepared using carbon particles as secondary template [34,35]. Mesoporous ZSM-5 exhibits increasing toluene conversion with increasing mesopore volume. A tentative explanation of differences

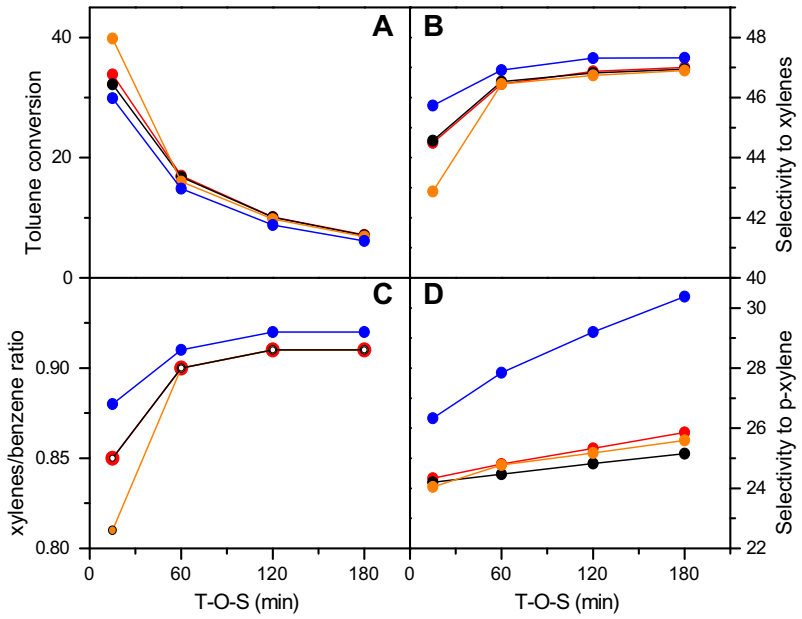

Fig. 6. Time-on-stream dependence of toluene conversion (A), selectivity to xylenes (B), xylene/benzene molar ratio (C) and *p*-xylene selectivity (D) in toluene disproportionation at 450 °C and WHSV = 20 h^{-1} for TUN (●), TUN/A (●), TUN/C (●) and TUN/G (●).

between mesoporous TUN and mesoporous MFI (albeit prepared by different procedures) might be in their different pore sizes. Slightly smaller pores of MFI (0.54 nm × 0.56 nm) invoke diffusional restrictions being much less important for TUN (0.52 nm × 0.60 nm).

Toluene conversions decreased from about 30–35% after 15 min of time-on-stream (T-O-S) to about 10% after 180 min for WHSV 20^{-1} and to about 20% for WHSV 2 h^{-1} most probably due to the coke formation. This was accompanied by a color change of the catalyst during the reaction. The lowest toluene conversion observed under all reaction conditions used was for TUN/G zeolites evidencing that narrowing of pores and plugging of some them is important for mass transport efficiency. This decrease in the toluene conversion was accompanied by an increase in the selectivity to xylenes, xylene/benzene molar ratio and *p*-xylene selectivity (Fig. 6B–D). Selectivity to xylene isomers reached about 46–48% at the reaction temperature of 450 °C and decreased to 44–45% at 500 °C. In parallel, we observed similar behavior of xylene/benzene molar ratio. At 450 °C xylene/benzene ratio was close to 0.9 while this values decreased to 0.8 at 500 °C as a result of the increased reaction rates of dealkylation and transalkylation reactions. Selectivity to *p*-xylene was close to 24–25% for TUN catalysts with exception of TUN and TUN/G. Parent TUN samples exhibited a slight increase in the *p*-xylene selectivity to about 26% after 180 min of T-O-S due to continuous deactivation by coke formation. In contrast, *p*-xylene selectivity over TUN/G, silylated samples, increased to 30.5% at 450 °C and 29.2% at 500 °C. Both values are after 180 min of T-O-S.

Reaction mechanism of toluene alkylation with C_3 alcohols or olefin having desorption and transport of products as the rate determining step was deeply investigated [36,37]. The kinetic and labelling studies over MFI and MEL zeolites provided clear evidence on the bimolecular transfer of propyl group from one reacting benzene ring to another one implicating the critical role of the zeolite structure. With TUN, the channel size of which zeolite is slightly larger than those of MFI and MEL, we wonder about the role of textural properties on conversions and selectivites. The toluene conversion after 15 min of time-on-stream (T-O-S) is influenced by toluene disproportionation, which is almost negligible after 55 min of T-O-S. For longer T-O-S values toluene conversion is close to 8% (toluene to isopropyl alcohol molar ratio is 9.6) for all TUN catalysts despite the way of modification (Figs. 7A and 8A). This confirms the importance of mainly desorption and/or diffusion of products in a similar way as for MFI catalyst although the channel size of TUN is slightly larger than that of MFI (0.52 nm × 0.60 nm vs. 0.54 nm × 0.56 nm). Based on the comparison of catalytic behavior of mesoporous TUN and MFI zeolites in toluene disproportionation, one can infer that differences in their pore sizes are much more significant for MFI zeolite. In contrast, when both zeolites are applied for the reaction, the rate of which is controlled by the product desorption (toluene alkylation with isopropyl alcohol [36]), catalytic behavior of both zeolites is rather similar and is not substantially changed by the presence of mesopores.

Cymenes are primary alkylation products and their selectivity increases with T-O-S at the extent of products of toluene disproportionation for shorter T-O-S and *n*-propyltoluenes for longer T-O-S (Figs. 7B and 8B). The highest selectivity to cymene was achieved for TUN and silylated TUN/G (80%) while all dealuminated and desilicated TUN catalysts showed lower cymene selectivity (50–70%) for T-O-S 180 min. Both dealumination and desilication led to a decrease in the selectivity to *p*-cymene. As the extent of dealumination was relatively low, *p*-cymene selectivity decreased from 80 to 70% after 180 min of T-O-S (Fig. 6D). In contrast, desilication creating large mesopores, resulted in *p*-cymene selectivities between 30 and 50% depending on the harshness of the treatment (Fig. 7D). In contrast, silylation of the external surface, TUN/G catalyst, enhanced *p*-cymene selectivity to about 85%. This finding points to the fact that the channel entrances are narrowed or partially plugged as a result of silylation preferring the *p*-cymene to leave easily the inner zeolite volume. This evidences that silylation of the crystals can enhance *para*-selectivity even for zeolites with channel dimensions slightly larger than those of MFI. The increase in *para*-selectivity can be explained in terms of a combination of both annihilation of acid sites on the external surface restricting consecutive and unselective reactions as well as by increasing differences in diffusion rates of individual cymene isomers. While the size of channels is increasing from MFI to TUN, which should decrease the differences among individual cymene isomers, it can be inferred that narrowing and partial plugging of channel entrances is critical for increasing *para*-selectivity.

Formation of undesired *n*-propyltoluenes leads to *iso*-/*n*-propyltoluene values about 3–7 for different TUN catalysts

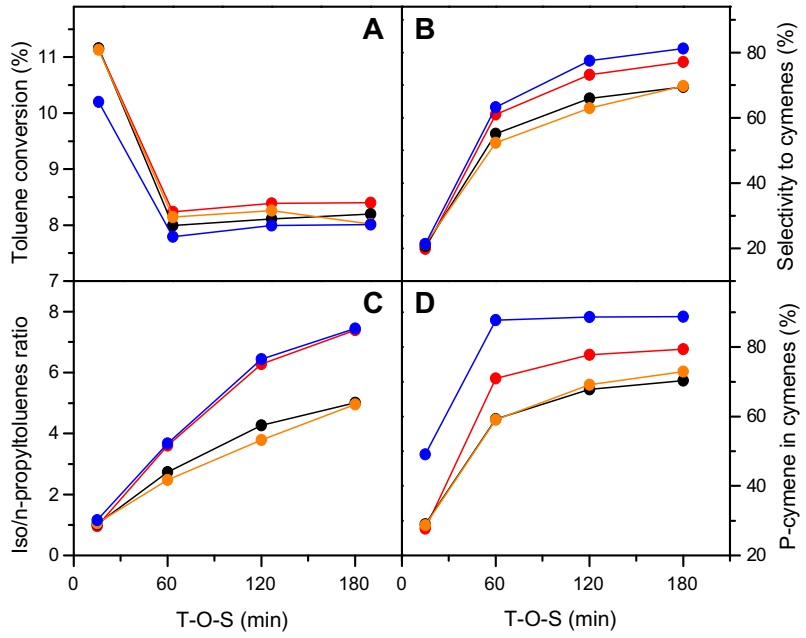

Fig. 7. Time-on-stream dependence of toluene conversion (A), selectivity to cymenes (B), *iso*-/*n*-propyltoluene ratio (C) and *p*-cymene selectivity (D) in toluene alkylation with isopropyl alcohol at 250 °C for TUN (●), TUN/A (●), TUN/C (●) and TUN/G (●).

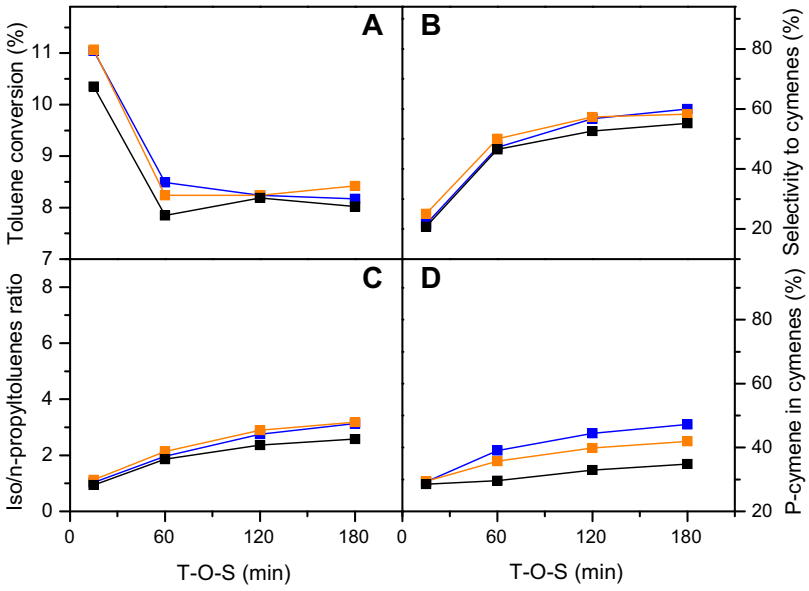

Fig. 8. Time-on-stream dependence of toluene conversion (A), selectivity to cymenes (B), *iso*-/*n*-propyltoluene ratio (C) and *p*-cymene selectivity (D) in toluene alkylation with isopropyl alcohol for TUN/D (■), TUN/E (■) and TUN/F (■).

(Figs. 7C and 8C). These values are slightly larger than for MFI zeolite [36], which is in agreement with a larger reaction volume in the channel intersections of TUN compared with MFI.

4. Conclusions

Post-synthesis treatment of parent TUN zeolite was carried out using dealumination, silylation and desilication procedures. These treatments and detailed characterization of acidic and textural properties of these zeolites resulted in:

1) no changes of the shape and size of TUN crystals as confirmed by SEM images,
2) the structure of TUN was preserved after all treatments and no significant changes were observed in the individual XRD patterns,
3) the decrease in the micropore volume by desilication, which was accompanied by a substantial increase in mesopore volume of TUN zeolites,
4) the increase in the concentration of Brønsted acid sites on the "external" surface of zeolites determined by the adsorption of 2,6-di-tert-butyl pyridine,
5) desilication resulted in a simultaneous decrease in the concentration of Brønsted acid sites and increase in the concentration of Lewis acid sited. This evidences that desilication procedure changes partially the type of acid sites,

6) toluene disproportionation, silylation of TUN zeolite provided a higher selectivity towards xylenes, higher xylene/benzene ratios as well as higher selectivity to *p*-xylene,
7) toluene alkylation with isopropyl alcohol, both dealumination and desilication decreased the selectivity to *p*-cymene,
8) the highest selectivity to *p*-cymene of about 90% was achieved on silylated TUN zeolite with a simultaneous increase in selectivity to cymenes.

The textural and catalytic results obtained in this study show that TUN zeolite is very interesting for transformation of aromatic hydrocarbons with a potential for other reactions of aromatic hydrocarbons.

Acknowledgements

The authors thank the Academy of Sciences of the Czech Republic for the support and M.K. thanks the Grant Agency of the Czech Republic for financial support (106/11/0819 and 203/08/H032).

References

[1] J. Čejka, A. Corma, S.I. Zones (Eds.), Zeolites and Catalysis: Synthesis, Reactions and Applications, Wiley-VCH, Weinheim, 2010.
[2] J. Čejka, B. Wichterlová, Catal. Rev. 44 (2002) 375.
[3] T.C. Tsai, S.B. Liu, I. Wang, Appl. Catal. A 181 (1999) 355.
[4] J. Čejka, S. Mintova, Catal. Rev. 49 (2007) 457.
[5] J. Perez-Ramirez, C.H. Christensen, K. Egeblad, C.H. Christensen, J.C. Groen, Chem. Soc. Rev. 37 (2008) 2530.
[6] J.C. Groen, J.C. Jansen, J.A. Moulijn, J. Perez-Ramirez, J. Phys. Chem. B 108 (2004) 13062.
[7] J.C. Groen, J.T. Sano, J.A. Moulijn, J. Perez-Ramirez, J. Catal. 251 (2007) 21.
[8] D. Verboekend, R. Caicedo-Realpe, A. Bonilla, M. Santiago, J. Perez-Ramirez, Chem. Mater. 22 (2010) 4679.
[9] A. van Miltenburg, J. Pawlesa, A.M. Bouzga, N. Žilková, J. Čejka, M. Stöcker, Top. Catal. 52 (2009) 1190.
[10] D. Verboekend, J.C. Groen, J. Perez-Ramirez, Adv. Funct. Mater. 20 (2010) 1441.
[11] Z. Musilová-Pavlačková, S.I. Zones, J. Čejka, Top. Catal. 53 (2010) 273.
[12] A. Jackowski, S.I. Zones, S.J. Hwang, A.W. Burton, J. Am. Chem. Soc. 131 (2009) 1092.
[13] S.I. Zones, A.W. Burton, K. Ong, US Patent 0148086 A1 (2007).
[14] E. Benazzi, J.L. Guth, L. Rouleau, US Patent 6,136,290 (2000).
[15] S.B. Hong, H.K. Min, Ch.H. Shin, P.A. Cox, S.J. Warrender, P.A. Wright, J. Am. Chem. Soc. 129 (2007) 10870.
[16] D. Xie, L.B. McCusker, C. Baerlocher, A.W. Burton, S.J. Hwang, T. Rea, K. Ong, S.I. Zones, Nat. Mater. 7 (2008) 631.
[17] C. Baerlocher, F. Gramm, L. Massüger, L.B. McCusker, Z. He, S. Hovmöller, X. Zou, Science 315 (2007) 1113.
[18] F. Gramm, Ch. Baerlocher, L.B. McCusker, S.J. Warrender, P.A. Wright, B. Han, S.B. Hong, Z. Liu, T. Ohsuna, O. Terasaki, Nature 444 (2006) 79.
[19] T. Odedario, S. Al-Khattaf, Appl. Catal. A 385 (2010) 31.
[20] A. Baduraig, T. Odedairo, S. Al-Khattaf, Top. Catal. 53 (2010) 1466.
[21] M.A. Bari Siddiqui, A.M. Aitani, M.R. Saeed, N. Al-Yassir, S. Al-Khattaf, Fuel 90 (2011) 459.
[22] M. Kubů, S.I. Zones, J. Čejka, Top. Catal. 53 (2010) 1330.
[23] J.C. Groen, L.A.A. Pfeffer, J.A. Moulijn, J.P. Ramirez, Micropor. Mesopor. Mater. 69 (2004) 29.
[24] C.A. Emeis, J. Catal. 141 (1993) 347.
[25] A. Zukal, H. Šiklová, J. Čejka, Langmuir 24 (2008) 9837.
[26] B. Gil, S.I. Zones, S.-J. Hwang, M. Bejblová, J. Čejka, J. Phys. Chem. C 112 (2008) 2997.
[27] A. Corma, V. Fornes, L. Forni, F. Marquez, J. Martinez-Triguero, D. Moscottiy, J. Catal. 179 (1998) 451.
[28] S. Zheng, H.R. Heydenrych, A. Jentys, J.A. Lercher, J. Phys. Chem. B 106 (2002) 9552.
[29] N. Žilková, M. Bejblová, B. Gil, S.I. Zones, A.W. Burton, C.-Y. Chen, Z. Musilová-Pavlačková, G. Košová, J. Čejka, J. Catal. 266 (2009) 79.
[30] J. Datka, B. Gil, J. Fraissard, P. Massiani, P. Batamack, Pol. J. Chem. 73 (1999) 1535.
[31] S.I. Zones, C.-Y. Chen, A. Corma, M.T. Cheng, C.L. Kibby, I.Y. Chen, A.W. Burton, J. Catal. 250 (2007) 41.
[32] J. Čejka, A. Krejčí, N. Žilková, J. Dědeček, J. Hanika, Microporous Mesoporous Mater. 44–45 (2001) 499.
[33] J. Čejka, A. Vondrová, B. Wichterlová, G. Vorbeck, R. Fricke, Zeolites 14 (1994) 147–153.
[34] Z. Musilová, N. Žilková, S.E. Park, J. Čejka, Top. Catal. 53 (2010) 1457.
[35] J.-B. Koo, N. Jiang, S. Saravanamurugan, M. Bejblová, Z. Musilová, J. Čejka, S.E. Park, J. Catal. 276 (2010) 327.
[36] B. Wichterlová, J. Čejka, J. Catal. 146 (1994) 523.
[37] I.I. Ivanova, D. Brunel, J.B. Nagy, E.G. Derouane, J. Mol. Catal. A 95 (1995) 243.